Materials Advances

ROYAL SOCIETY OF CHEMISTRY

PAPER

View Article Online
View Journal | View Issue

Cite this: *Mater. Adv.*, 2022, 3, 373

Cu-ion-induced n- to p-type switching in organic thermoelectric polyazacycloalkane/carbon nanotubes†

Shinichi Hata, *[a] Riku Nakata,[a] Soichiro Yasuda,[a] Hiroki Ihara,[a] Yukou Du,[b] Yukihide Shiraishi *[a] and Naoki Toshima[c]

The design and scale-up of carbon nanotube (CNT)-based thermoelectric (TE) modules is limited by the low structural similarity between p-type enhancers and n-dopants. This study was aimed at investigating the organic TE properties of polyazacycloalkane/CNT TE films prepared using the drop casting method and the effect of Cu ion doping that can coordinate with its organic ligands. The Seebeck coefficient of cyclen-doped CNTs was −43.3 μV K^{-1} at 345 K but reduced to 41.6 μV K^{-1} after adding Cu ions. Cu ion addition switched the charge carrier type of the composite film from electrons to holes owing to cyclen complexation with Cu ions, resulting in a neutral molecular state with suppressed electron donation of the dopant molecules. Notably, conventional approaches cannot maintain sufficient power characteristics owing to the reduced electrical conduction induced by structural defects in the nanotubes. However, herein, an output power exceeding 200 μW m^{-1} K^{-2} was obtained, which was 2–5 times higher than that of existing carrier-switchable CNTs. For a typical TE module consisting of five pairs of p-type (Cu(II)-cyclen/CNT)-n-type (cyclen/CNT) junctions, the generated TE voltage and power, depending on the temperature gradient, were similar to the theoretical values. Under optimized conditions, a maximum output power of 1.36 μW was achieved at a temperature difference of 75 K, which is higher than that of previously reported carrier-switchable CNT-based TE modules that used oil-based dopants, whereas we used optimal water-soluble dopants. The proposed approach can help simplify the path from material preparation to module fabrication.

Received 22nd September 2021,
Accepted 31st October 2021

DOI: 10.1039/d1ma00871d

rsc.li/materials-advances

Introduction

At present, more than 72% of the primary fossil fuel energy is lost as waste heat worldwide, with significant losses incurred in vehicles, plants, and thermal power plants.[1,2] Fossil fuel energy loss is a critical problem associated with energy use, and effective recycling of this waste heat is critical to achieving a sustainable society. Carbon nanotube (CNT)-based materials, such as films,[3–5] mats,[6] and yarns,[7] can be used to directly convert heat into electricity and recover energy from waste heat at low temperatures.[8–10] In this manner, such materials can enhance energy utilization and help satisfy the demand for sustainable energy conversion technologies.[11–14] These materials exhibit unique advantages over inorganic materials such as high flexibility, lightweight, nontoxicity, material abundance, and scalability of manufacturing processes,[15–17] including large-area solution processing. Therefore, such materials can promote the realization of a series of novel thermoelectric (TE) applications such as power generation for the Internet of Things,[18] wearable heating and cooling devices,[19] and biomedical implants.[20] Notably, in-plane thermal conductivity measurements of freestanding films made of CNTs or conductive polymers are challenging in thin films owing to the unfavorable heat flow.[21,22] The corresponding conversion efficiency can be estimated using the thermal power factor (PF):

$$PF = S^2\sigma, \quad (1)$$

where S and σ denote the Seebeck coefficient ($S > 0$ and $S < 0$ for p- and n-type semiconductors, respectively) and electrical conductivity, respectively.

TE modules can be prepared by interconnecting a single type of TE material with ordinary conductors. However, in this case, only half of the legs generate thermal voltage. Notably, in such frameworks, p-type materials are preferred over n-type materials owing to their lower stability in the atmosphere.[16,23]

[a] *Department of Applied Chemistry, Faculty of Engineering, Sanyo-Onoda City University, Daigaku-dori, 1-1-1, Sanyo-Onoda, Yamaguchi 756-0884, Japan. E-mail: hata@rs.socu.ac.jp, shiraishi@rs.socu.ac.jp*
[b] *College of Chemistry, Chemical Engineering and Materials Science, Soochow University, Suzhou 215123, P. R. China*
[c] *Professor Emeritus, Tokyo University of Science Yamaguchi, Japan*

† Electronic supplementary information (ESI) available. See DOI: 10.1039/d1ma00871d

More efficient devices can be prepared by alternately connecting p-type and complementary n-type materials in an electrical series framework. In general, CNTs usually exhibit a positive Seebeck coefficient and p-type behavior owing to oxygen doping in the air.[24] To prepare such a module, a dispersant or molecular enhancer, such as sodium dodecyl benzene sulfonate,[4] polyaniline,[12] poly(3,4-ethylenedioxythiophene)–poly(styrenesulfonate),[13] or poly(Ni-ethenetetrathiolate),[25] must be used to enhance p-type CNTs. Moreover, a molecular dopant that can easily induce CNT carriers from holes to electrons in air, such as cobaltocene,[26] crown ether complex,[27] polyethyleneimine (PEI),[28] and poly(vinyl alcohol),[29] must be prepared. In the existing frameworks, these processes were implemented by controlling the electronic state (Fermi level or work function) of the CNTs. Considerable research was conducted using molecular compounds with different electrical and chemical properties but low structural correlations.[30,31] In addition, in the most widely used conventional method to prepare TE CNTs, which involves filter-deposited bucky paper, the resulting film was cut to a specific size and then impregnated with a highly concentrated molecular enhancer/dopant solution in an organic solution such as alcohol[4] or dimethyl sulfoxide[32] to create doped CNTs. In such scenarios, the intrinsic advantages of solution-processable organic materials, such as printing compatibility, which is critical for large-scale applications, cannot be exploited. To address this problem, it is desirable to formulate a doping strategy that can simplify the fabrication of p- and n-type paired TE modules.

Some researchers have indicated that the UV irradiation of organic solvent deposits containing poly(3-hexylthiophene)/CNTs corresponded to a switch from p- to n-type (Seebeck coefficient from $\sim$25 to ~ -10 μV K^{-1}) and demonstrated the possibility of photopatterning the n-type region in the p-type film.[33] Others have highlighted the feasibility of controlling the n-doped state (Seebeck coefficient from 125 to -80 μV K^{-1}) *via* the ammonia plasma treatment of semiconducting CNT films.[34] However, in these methods, the electrical conductivity of the nanotubes is considerably reduced owing to the severe physical damage of the film, and sufficient TE power cannot be achieved; in the abovementioned studies, the PF value after carrier conversion was less than 100 μW m^{-1} K^{-2}. Systematic research on carrier-switchable CNTs to expand the applications of CNT-film-based TE modules remains limited owing to several practical challenges. In particular, it is necessary to identify appropriate dopants to facilitate solution-processable doping processes and investigate the organic TE properties of relevant materials to simplify the fabrication of p- and n-type paired TE modules.[35,36]

Accordingly, this study aimed to formulate a novel switching mechanism to control the carrier-type in CNTs with organic TE properties using a water-based drop-casting technique that can be adapted to printing techniques. Specifically, the TE properties of CNTs complexed with polyazacyclic alkane compounds and the changes in carrier properties caused by the supramolecular interactions between metal ions and polyazacyclic alkanes were examined. Amine-derivatives, such as 1,4,7,10-tetraazacyclododecane (cyclen), are electron-rich and water-soluble organic molecules with multiple lone electron pairs on multiple N atoms.[37,38] In other words, such materials are excellent electron-donating molecules that can carefully encapsulate nanotubes and increase the electron concentration. Nevertheless, the dopant functionality of such materials has not received adequate attention. The doping of nanotubes with polyamines delays the n-type degradation caused by atmospheric oxygen and water and yields chemically superior n-type materials in aqueous environments. In addition, macrocyclic amines of polyazacycloalkanes act as scaffolds for incorporating Cu ions into molecular fragments.[39] This unique property can help control the dopant function based on the change in the electron-donating nature of the intramolecular N atoms, thereby modifying the TE properties of the nanotubes.

Herein, we investigated the effect of the electron-donating ability of the dopant on the nanotubes, the switching of the corresponding carriers, and the organic TE behavior corresponding to the coordination and chemical molecular function of Cu ions. In addition, TE modules were fabricated using CNT films to which Cu ions were introduced to control the carriers. The electrical properties of these devices were investigated with respect to temperature. A doping strategy that could reduce the processing complexity and facilitate complex additive printing processes to enhance the efficiency and simplify module fabrication was proposed.

Experimental

Materials

Single-walled CNTs (Product ID EC1.5, purity >90%, diameter: 1.5 ± 0.8 nm, metal : semiconductor composition = 1 : 2) were obtained from Meijo Nano Carbon Co. Ltd, Aichi, Japan. 1,4,7,10-Tetraazacyclododecane (cyclen), 1,4,8,11-tetraazacyclotetradecane (cyclam), and copper(II) nitrate trihydrate were purchased from Fujifilm Wako Pure Chemical Corp., Japan. Triazacyclononane (TACN) was obtained from Tokyo Chemical Industry Co., Ltd, Japan. Polyimide substrates were supplied by UBE Industries, Ltd, Japan. All the materials were used as received without purification. Ultrapure water (specific resistance: 18.2 MΩ cm at 298 K) was used in all experiments.

Preparation of the cyclen/CNT and Cu(II)-cyclen/CNT films

Fig. 1 schematically illustrates the preparation of the TE film. The cyclen/CNT film was prepared using the following procedure. First, 6.0 mg of CNTs was added to 6.0 mL of 8.33 mM aqueous cyclen solution in a 13.5 mL screw tube. The mixture was stirred using an ultrasonic homogenizer (Ultrasonic Cleaner, TAITEC; Branson Sonifier 250D, Central Scientific, Tokyo, Japan) for 5 min while cooling in an ice bath (as the reaction was exothermic). The homogeneous cyclen/CNT solution (3.0 mL) was drop-cast onto a polyimide sheet (5 × 3 cm) and placed on a hot plate at 333 K for 1 h. To promote film formation, 2.0 mL of the homogeneous CNT solution was cast

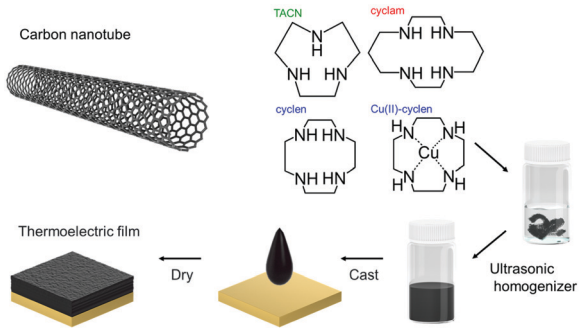

Fig. 1 Schematic of the fabrication of a molecule-doped CNT film. The nanotubes are dispersed in an aqueous solution of each molecule by using an ultrasonic homogenizer. The dispersion is cast and dried on a polyimide substrate followed by the preparation of the CNT-based thermoelectric film.

and dried at 333 K for 5 h and at 383 K for 30 min to produce a dry cyclen/CNT film. The TACN/CNT and cyclam/CNT films were prepared using this method. To obtain the Cu(II)-cyclen/CNT films, an 8.33 mM Cu(II)-cyclen aqueous solution, prepared by admixing the aqueous cyclen solution with an aqueous copper nitrate trihydrate solution, was used as the solvent for the nanotubes. The CNT composite layer on the polyimide sheet was 5.0 ± 1.0 μm thick. Notably, the prepared film was more than 100 nm thick, and the TE performance was observed to be independent of the CNT film thickness.[36] Details of the structural analysis of the film are provided in the ESI.†

Fabrication and evaluation of the TE module

We alternately attached five Cu(II)-cyclen/CNT (p-type) and five cyclen/CNT (n-type) TE elements, each with a width and length of 6.0 and 0.5 cm, respectively, to a polyimide paper substrate. A silver paste was prepared to fabricate a bar-coated conductive electrode film. The paste also functioned as a conductive adhesive to form electrical connections between the electrode and TE elements. The hot end of the device was placed on a heating table to achieve a temperature difference in the range of 15–75 K between the two ends of the device; the temperature difference was recorded using a data acquisition and logging multimeter system DAQ6510/7700 (Keithley Instruments Inc., USA). The device performance was evaluated using a 2450, 2182 A J^{-1} voltage detector (Keithley Instruments Inc., USA).

Results and discussion

Fig. 2 summarizes the S, σ, and PF values of the polyazacycloalkane/CNT films at 345 K. The S value of the original CNTs was 62.7 μV K^{-1}, indicating that CNTs with p-type properties were obtained owing to aerobic oxidation, consistent with previous results.[40] The Seebeck coefficients of the TACN, cyclen, and cyclam/CNTs were −42.2, −43.3, and −46.4 μV K^{-1}, respectively. In contrast to the pure CNT films, the polyazacycloalkane-doped CNT films exhibited negative Seebeck coefficients regardless of the change in the number of N atoms and hydrocarbons in their molecular backbone. The key to n-type doping is the electron

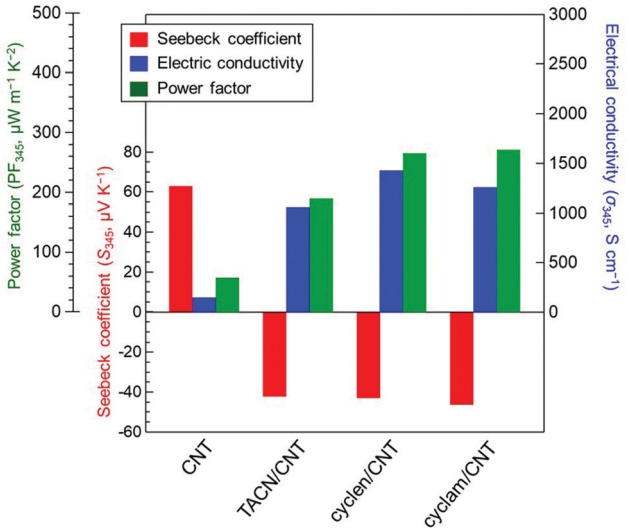

Fig. 2 In-plane thermoelectric properties of polyazacycloalkane/CNT films. The measurements were performed at 345 K in a He atmosphere.

transfer between the dopant and the CNTs. The Seebeck coefficient has been reported to be extremely sensitive to the solvent used in the doping process. Nitrogen-containing solvents such as *N*,*N*-dimethylformamide[41] and *N*-methylpyrrolidone[42] exhibit a negative Seebeck coefficient and increase the output of n-type doping owing to the electron-donating ability of N atoms. In this study, water was used in the preparatory solvent, and thus, the unexpected doping could not occur. In general, the n-doping of CNTs involves the adsorption of polyazacycloalkanes onto the nanotube surface; the N atoms function as primary electron donors, causing an upward shift in the nanotube Fermi energy. This n-formation mechanism is consistent with the behavior of films doped with nitrogen or phosphorus organic compounds.[30] Additionally, in n-type CNTs, water participates in electrophilic reactions with the electron-activating sites, causing the doping level and Seebeck coefficient of n-type CNTs to revert to those of air-exposed CNTs.[16,23] In this study, it was noted that electron-rich dopants may protect CNTs and prevent harmful reactions between the electronically active sites of the nanotubes and water. However, the σ value of pure CNTs was low (148 S cm^{-1}) due to the absence of dispersants. In contrast, the σ values of the TACN/CNT, cyclen/CNT, and cyclam/CNT were 1057, 1423, and 1259 S cm^{-1}, respectively. This phenomenon occurred because the polyazacycloalkanes functioned not only as dopants to increase the electron concentration of the nanotubes but also as dispersants. Consequently, in accordance with the trend of S values, the PF values of the cycloalkane-doped CNT films exhibited the following decreasing order: cyclam (272 μW m^{-1} K^{-2}) > cyclen (266 μW m^{-1} K^{-2}) > TACN (190 μW m^{-1} K^{-2}). These results were comparable to those obtained using small synthetic organic molecules (acridine[43] and imide compounds[44]), which endowed CNTs with effective n-type PF values. These findings show that simple polyazacycloalkanes are promising dopants for CNTs that exhibit high n-type PF values. Furthermore, conventional n-type doping of

CNTs in an aqueous solution involves a pH limitation,[45] which impedes the doping process. This limitation is effectively eliminated in the proposed experimental method. Moreover, the proposed approach is an economically viable solution as it is environmentally friendly and does not use organic solvents.

To investigate the surface properties, N_2 adsorption isotherms were obtained at 77 K. The properties of the N_2 adsorption isotherms of pristine CNTs (Fig. 3(a)) were similar to those of mesoporous materials;[46] however, those of polyazacycloalkane/CNTs were considerably different, with only a slight increase even in the high relative pressure region ($0.9 < P/P_0 < 1.0$). In the low relative pressure region ($0 < P/P_0 < 0.4$), the doped CNT sample did not adsorb a significant number of N_2 molecules compared to the pristine sample (Fig. 3(b)). This finding suggests that the affinity between the CNT surface and adsorbed N_2 disappears in the presence of polyazacycloalkanes. The apparent N_2 specific surface areas of the pristine, TACN, cyclen, and cyclam/CNTs calculated using the Brunauer–Emmett–Teller (BET) method were 485.3, 38.7, 50.2, and 42.1 $m^2\ g^{-1}$, respectively. The series of N_2 adsorption isotherms and BET specific surface area values clearly show that the polyazacycloalkanes seal the nanotube surface.[47]

The Raman spectra of the samples clarified the structure of the nanotubes, interactions between the added dopants and CNTs, and structural changes after n-type doping. In the extended region of the radial breathing mode (RBM) band, the addition of polyazacycloalkanes reduced the intensity of the original CNT peak (Fig. 4(a)). The absorption of n-type dopants on the CNT surface led to interference with the radial carbon atom vibration; this phenomenon has also been reported for PEI-doped CNT composites.[48] In other words, owing to the decrease in the intensity due to doping in the RBM band, the molecules attached to the CNT surface coating the carbon atoms and suppressed their radial vibration. Fig. 4(b) shows the normalized spectrum of the G-band associated with the vibrations of the carbon atoms along the nanotube plane. After polyazacycloalkane doping, the G-band of the CNTs shifted slightly from 1590 cm^{-1} to the lower frequency side. This behavior indicated that electron doping occurred from polyazacycloalkanes to CNTs.[49] The Raman D/G ratios, which indicate the crystallinity of the nanotubes, were determined to be 0.009, 0.009, 0.010, and 0.010 for the pristine, TACN, cyclen, and cyclam/CNTs, respectively. The doping process did not introduce any structural defects, and no change was observed in the D band. These findings indicate that the non-covalent adsorption of polyazacycloalkanes onto the CNTs is the trigger for the electron transfer from the dopants to the CNTs. Specifically, the polyazacycloalkane-based compounds considered in this study involve water-soluble dopants that change the state of CNTs to the n-state.

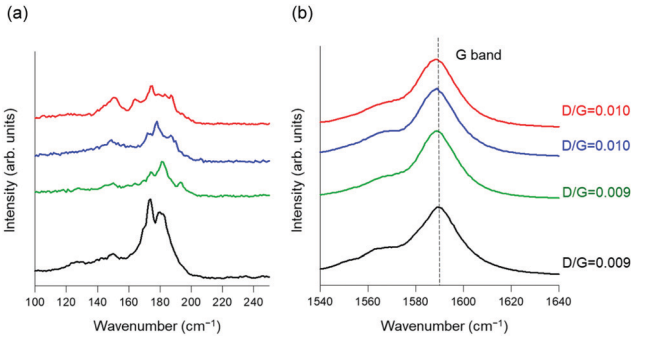

Fig. 4 Normalized Raman spectra (a) in the low-frequency radial breathing mode range and (b) at the G-band. Color code: CNT, black; cyclam/CNT, red; cyclen/CNT, blue; TACN/CNT, green.

To investigate the effect of Cu ion addition on the TE properties of nanotubes, the complexation state of cyclen, as a classical polyazacycloalkane, in the solution was preliminarily investigated. As shown in Fig. S1(a) (ESI†), when Cu ions were added in an equimolar manner, the aqueous cyclen solution changed from clear and colorless to a blue solution with maximum absorption at 588 nm. According to the Job-plot method[50] (Fig. S1(b), ESI†), which determines the empirical ratio of the reactants in chemical equilibrium, the mole fraction at maximum absorbance was 0.5 (Fig. S1(c), ESI†). Therefore, the chemical species formed complexes in a 1:1 stoichiometric ratio.[51] The four nitrogen atoms in the ring of the cyclen molecule functioned as donor atoms and formed a coordinating covalent bond that efficiently bonded with the Cu ion.[52]

Furthermore, doped CNT films were fabricated using cyclen (Cu(II)-cyclen) aqueous solution with equimolar Cu ion addition. To determine the change in the film formation state before and after Cu ion addition, the surfaces of the samples were photographed, and the surface morphology was evaluated *via* scanning electron microscopy (SEM, Fig. 5(a)–(c)). A visual

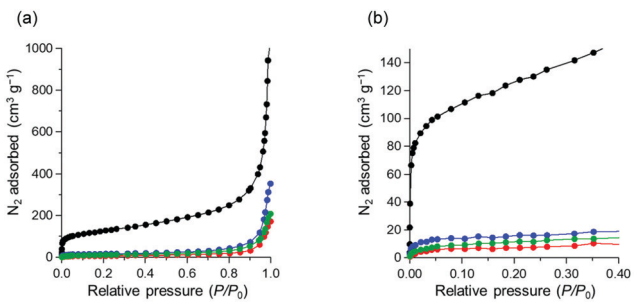

Fig. 3 N_2 adsorption isotherms at 77 K: (a) wide range and (b) narrow range; color code: CNT, black; cyclam/CNT, red; cyclen/CNT, blue; TACN/CNT, green.

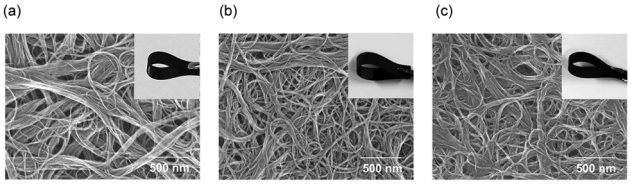

Fig. 5 Scanning electron microscopy (SEM) images of the surfaces of (a) pristine CNT, (b) cyclen/CNT, and (c) Cu(II)-cyclen/CNT films with corresponding photographs shown in the insets.

observation indicated that the film was flexible before and after Cu ion addition and did not lose its shape when bent. Moreover, the nanotube layer was fixed to the polyimide substrate. In the SEM image of pristine CNTs, rope-like nanotube bundles bound by van der Waals forces could be observed,[53] indicating a film structure with numerous cavities and voids. In contrast, the morphology of the cyclen/CNT and Cu(II)-cyclen/CNT films involved a continuous dense network of randomly oriented nanotubes. The bundle widths of pristine, cyclen/CNT, and Cu(II)-cyclen/CNT were 71.4 ± 32.4, 33.9 ± 16.8, and 36.9 ± 19.3 nm, respectively, indicating that cyclen or Cu(II)-cyclen functioned as a dispersing agent for CNTs. Both diluted drop-casting solutions were observed by transmission electron microscopy (TEM) to indirectly determine the dispersion properties of the molecular cyclen and Cu(II)-cyclen on the nanotubes. Cyclen or Cu(II)-cyclen was randomly distributed on the surface of both the CNT bundles and the nanotubes themselves, which have a hair-like appearance, as shown in Fig. S2 (ESI†), as can clearly shown in the TEM images. This morphological observation is direct evidence that cyclens were adsorbed on the nanotubes, regardless of the addition of Cu ions.

The S, σ, and PF values of the cyclen and Cu(II)-cyclen/CNT films for the temperature range (T, 330–380 K) are shown in Fig. 6(a)–(c), respectively. Cyclen/CNT films exhibited negative S values at all temperatures, owing to which, no obvious thermal degradation occurred. Moreover, the films behaved as n-type semiconductors with electron carriers. As the temperature increased, the S value gradually decreased from −41.0 μV K^{-1} at 300 K to −48.1 μV K^{-1} at 380 K. In contrast, the Cu(II)-cyclen/CNT film has a positive S value, corresponding to a p-type semiconductor with hole carriers. This phenomenon was also observed in the TACN and cyclam systems (Fig. S3, ESI†). In other words, the n- to p-type conversion of polyazacycloalkane/CNT was achieved in the presence and absence of Cu ions, independent of the measurement temperature. Similar to the case before Cu ion addition, the S value of Cu(II)-cyclen/CNTs increased with increasing temperature, from 41.0 μV K^{-1} at 300 K to 44.3 μV K^{-1} at 380 K. Notably, the trend of the σ value for both samples was opposite to that of the S value. The negative slope of the σ–T line decreased with increasing temperature regardless of the presence of Cu ion, and the samples exhibited metal-like transport properties.[54] This finding indicates that the formed nanotube network, as observed in the SEM image, involved a bypass that could transport charge carriers. Moreover, the bonding between the CNT bundles of the matrix material was strong even when Cu ions were added. According to the results of the S and σ values, the maximum PF values of cyclen/CNT and Cu(II)-cyclen/CNT were p-type 293 μW m^{-1} K^{-2} and n-type 234 μW m^{-1} K^{-2} at 380 K, respectively.

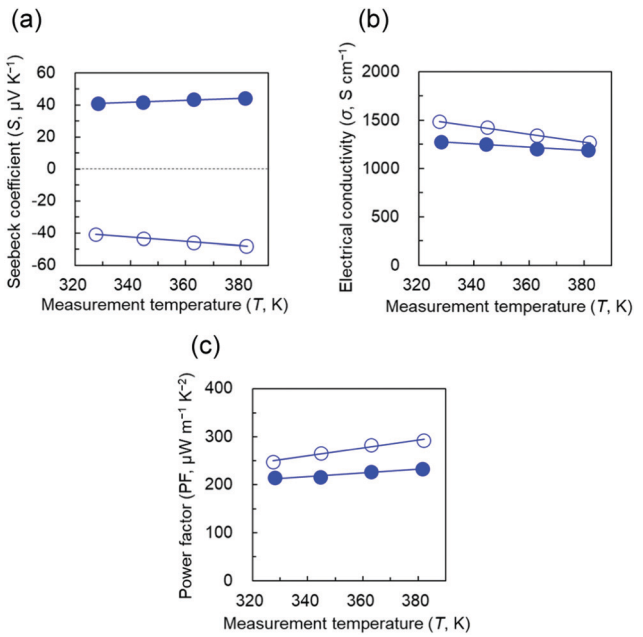

Fig. 6 (a) Seebeck coefficient, (b) electrical conductivity, and (c) PF of cyclen/CNT (open circle) and Cu(II)-cyclen/CNT (closed circle) as functions of temperature.

The structure of the composite film was extensively examined to determine the role of Cu(II)-cyclen. In the low relative pressure region ($0 < P/P_0 < 0.4$) in the N_2 adsorption isotherms of Cu(II)-cyclen/CNT and cyclen/CNTs, almost no adsorption of N_2 molecules was observed compared to that in the pristine case (Fig. S4, ESI†). In addition, according to the Raman measurement results, the intensity decreased owing to doping in the RBM band in the Cu(II)-cyclen/CNT, as in the case of cyclen/CNT (Fig. S5(a), ESI†). Furthermore, the G-band position of Cu(II)-cyclen/CNT was 1590 cm^{-1}, similar to that of pristine CNT. This finding indicates that the n-doping effect of cyclen on the nanotubes was eliminated with Cu ion addition (Fig. S5(b), ESI†). The Raman D/G ratio did not indicate the occurrence of significant structural defects. In general, CNTs have a large specific surface area, and their carriers are highly sensitive to the additive/atmospheric conditions associated with the film.[55,56] Overall, the extreme change in carrier properties can likely be attributed to the electron donation of polyazacycloalkanes on the nanotube surface being blocked by Cu ion complexation. In other words, Cu(II)-cyclen, a charge-neutral molecule, may serve as a p-type enhancer that acts as a dispersant for the nanotubes. To fabricate practical TE devices, both n- and p-type materials with large PF values must be used. Existing approaches involve ammonia plasma treatment of CNT-filtered bucky paper or UV light irradiation induction during conjugated polymer/CNT solution deposition. In these frameworks, although the carriers can be converted, the damage to the nanotubes caused by doping results in a small σ value (leading to a small PF value).[33] In the proposed approach, the carrier conversion of CNTs is based on the change in the chemical property of the dopant by metal ions, and thus, the physical damage to the nanotubes is minimized.[31] In other words, carrier control of the CNTs can be realized by switching the electron-donating ability of the dopant triggered by the metal ion, without sacrificing the electrical conductivity of the material. Consequently, the system records PF values >200 μW m^{-1} K^{-2} for both p- and n-type

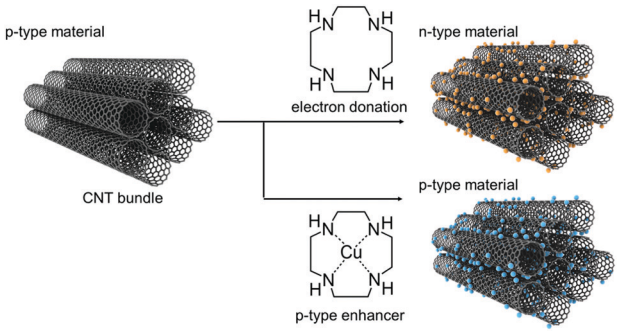

Fig. 7 Schematic of switching carrier types of CNTs using cyclen and Cu(II)-cyclen. Cyclen is a water-soluble dopant that changes the state of the nanotubes to the n-state. Cu(II)cyclen/CNT acts as a nanotube dispersant. Cyclen is an electron donor to nanotubes, although this potency is lost through Cu ion complexation.

transport, thereby outperforming other carrier-switchable CNT-based films (Fig. 7). Notably, the S value of cyclen/CNTs remained almost at its initial value for 14 days in air at room temperature (298 K and 60% RH) (Fig. S6, ESI†). Doping with electron-rich dopants such as cyclen has been suggested to be effective not only for synthesizing n-type CNTs but also for maintaining their n-state. The proposed approach can thus promote the development of scalable TE devices and simplify the fabrication processes.

We evaluated the TE performance of flexible devices made of cyclen/CNT (n-type) and Cu(II)-cyclen/CNT (p-type). As shown in Fig. 8(a) and Fig. S7 (ESI†), the device consisted of five n-type legs and five p-type legs, alternately connected in series on a polyimide substrate. Each leg had a width of 0.5 cm and a length of 6.0 cm. The hot end of the device was heated using a heating plate, and the cold end was exposed to air. The temperatures of the hot (T_{hot}) and cold (T_{cold}) ends were monitored using a data acquisition and logging multimeter system. The temperature difference ΔT (= $T_{hot} - T_{cold}$) was controlled by adjusting the temperature of the heating plate. Fig. 8(b) compares the real voltage (V_{AC}) and theoretical voltage (V_{TH}) of the TE module for each value of ΔT. V_{TH} was calculated as follows:[57]

$$V_{TH} = (N_p S_p + N_n S_n)\Delta T, \quad (2)$$

where N and S are the number and Seebeck coefficient of the p- and n-type CNT films, respectively. V_{AC} increases with the increasing temperature gradient, indicating a linear relationship, and its value is similar to the V_{TH} value at ΔT = 60 K. The maximum V_{AC} value is 19.3 mV, which is 75.8% of the V_{TH} value. This finding indicates that this material can be applied to the module while yielding a satisfactory Seebeck effect. The current–voltage power curve at ΔT = 15–75 K is shown in Fig. 8(b). As the temperature gradient increases, the obtained power output and current output increase. The maximum output power (P_{AC}) at ΔT = 15, 30, 45, 60, and 75 K is approximately 0.02, 0.15, 0.42, 0.79, and 1.36 μW, respectively (Fig. 8(c)).

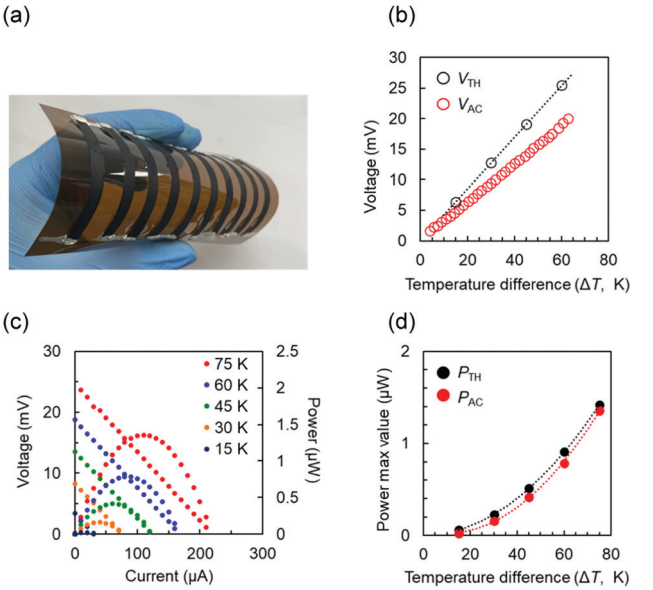

Fig. 8 (a) Digital photograph of the five-unit p–n device exhibiting a high flexibility. (b) Voltage generated as a function of the steady-state temperature difference between the two ends of the device, where V_{TH} is the theoretical voltage and V_{AC} is the actual voltage of the assembled device. (c) Output power–output current and output voltage–output current curves of the device at temperature differences of 15, 30, 45, 60, and 75 K between the two ends. (d) Variation in the maximum values of theoretical (P_{TH}) and actual (P_{AC}) output power with temperature difference (ΔT) between the hot and cold junctions of the device.

The theoretical output power (P_{TH}) was calculated as follows:[43]

$$P_{TH} = V_{TH}^2/4R_i, \quad (3)$$

where R_i is the internal resistance of the fabricated p–n device (179 Ω). The P_{AC} values at ΔT = 15, 30, 45, 60, and 75 K were in agreement with the P_{TH} values calculated using eqn (3). (Fig. 8(d)) In general, commercially available TE modules consist of hundreds of p–n couples. The electrical characterization results indicate that with certain advancements, flexible TE modules with a considerably higher power or cooling capability can be obtained.

Table S1 (ESI†) summarizes the preparation and properties of p- and n-type paired TE modules composed of organic or organic/inorganic composites of devices similar to that used in this study.[43,58–66] Recently, TE modules were prepared using the same dopants (benzothienobenzothiophene-charge transfer complex[59] and naphthalene diimide derivatives[60]) for p- and n-type materials. However, in these systems, effective n-doping with the preparation solvent triethylamine was essential for n-type materials. In addition, in order to control the carrier type, the dopants investigated so far are mostly oil-soluble compounds with almost no structural similarity and high-boiling-point organic solvents (dimethyl sulfoxide,[43] *N*,*N*-dimethylformamide,[62] and *N*-methylformamide[64]), or they had to be dissolved in an aqueous alcohol solution.[58,65,66] The different processes for suitable carrier control are very

troublesome in the design and scale-up of CNT-based TE modules.[31] In the cyclen/CNT-based TE module prepared in this study, Cu ions can easily switch n-type materials to p-type materials, and the carrier types that make up the CNTs can be controlled *via* the same process using aqueous solvents. The fabricated device can generate electric power in the μW-order. These results show great potential to simplify the basic-to-manufacturing journey of p- and n-type paired TE modules. Thus, this work shows an implementation of p- and n-type paired TE modules using a green route that can overcome the significant drawbacks of previous studies.

Conclusions

We prepared n-type CNT-based TE materials by coating nanotube surfaces with supramolecular compound polyazacycloalkane molecules. This method involved the use of water, which is traditionally undesirable in the preparation of n-type materials. The proposed method is implemented through drop-casting, which is compatible with printing processes for large-scale applications. The added electron-rich dopants donate electrons to the CNTs while preventing detrimental reactions between the nanotubes and water. Furthermore, Cu ion trapping in the coordination sites of polyazacycloalkanes suppresses the electron donation from the dopants to the nanotubes. Consequently, the carrier properties of the polyazacycloalkane/CNT TE film are switched from n- to p-type through Cu ion addition. Using this approach, the cyclen system records PF values >200 μW m^{-1} K^{-2} for both p- and n-type transport, thereby outperforming existing carrier-switchable CNT-based films. This phenomenon is only possible with tubular molecules that have trapping sites. Linear molecules, such as triethylenetetramine, have weak coordination forces with metal ions, and therefore, it may not be possible to accurately control their properties. This novel strategy can achieve high PF values in TE films without introducing structural defects in CNTs. Notably, this strategy represents a valuable application of dopant/nanotube interface engineering based on chemical interactions. In addition, a typical TE module incorporating five legs each of n- and p-type alternately generates TE voltage, which varies linearly with the temperature gradient. At $\Delta T = 75$ K, the power is of the order of several microwatts. This TE module, fabricated through a simple process, is a promising power source for large area environmental power applications.

Future work could examine the electronic structure and electrical transport properties, such as the carrier concentration and mobility associated with the Cu-ion-induced n- to p-type switching in polyazacycloalkanes/CNTs. For the fabrication of compact wearable devices, planar structure TE modules are preferable to π-shape structures because of their higher power density. In the future, it would be possible to simplify the conventional TE module fabrication by treating large area cyclen/CNT films with Cu ion solution to create high precision patterns of successively repeated p-type and n-type regions. The proposed method can serve as a key technology to fabricate carrier-switchable CNT-based materials to facilitate the realization of an environmentally sustainable society.

Author contributions

S. H. and Y. S. conceived the original concept and designed the experiments. S. H. wrote the manuscript. S. H. and R. N. performed the material synthesis and characterization. S. Y. and H. I. supported the analysis of the results. Y. D. and N. T. provided advice regarding the interpretation of the results. S. H. and Y. S. supervised the project. All authors contributed to the discussion of the results.

Conflicts of interest

The authors declare that they have no known competing financial interests or personal relationships that could have influenced the work reported in this paper.

Acknowledgements

This study was supported in part by KAKENHI projects (No. 21K14428 to S. H. and 19K05633 to Y. S.) from the JSPS, Hitachi Metals and Materials Science Foundation, Japan.

Notes and references

1 C. Forman, I. K. Muritala, R. Pardemann and B. Meyer, *Renewable Sustainable Energy Rev.*, 2016, **57**, 1568–1579.
2 A. S. Rattner and S. Garimella, *Energy*, 2011, **36**, 6172–6183.
3 H. Romero, G. Sumanasekera, G. Mahan and P. Eklund, *Phys. Rev. B: Condens. Matter Mater. Phys.*, 2002, **65**, 205410.
4 C. K. Mytafides, L. Tzounis, G. Karalis, P. Formanek and A. S. Paipetis, *ACS Appl. Mater. Interfaces*, 2021, **13**, 11151–11165.
5 S. Horike, Y. Kuwahara, Q. Wei, K. Kirihara, M. Mukaida and T. Saito, *Appl. Phys. Lett.*, 2021, **118**, 173902.
6 Q. Hu, Z. Lu, Y. Wang, J. Wang, H. Wang, Z. Wu, G. Lu, H.-L. Zhang and C. Yu, *J. Mater. Chem. A*, 2020, **8**, 13095–13105.
7 J. Choi, Y. Jung, S. J. Yang, J. Y. Oh, J. Oh, K. Jo, J. G. Son, S. E. Moon, C. R. Park and H. Kim, *ACS Nano*, 2017, **11**, 7608–7614.
8 Z. Liu, X. Wang, S. Wei, H. Lv, J. Zhou, P. Peng, H. Wang and G. Chen, *CCS Chem.*, 2021, **3**, 2040–2414.
9 Y. Zhang, Q. Zhang and G. Chen, *Carbon Energy*, 2020, **2**, 408–436.
10 X. Li, K. Cai, M. Gao, Y. Du and S. Shen, *Nano Energy*, 2021, **89**, 106309.
11 C. Meng, C. Liu and S. Fan, *Adv. Mater.*, 2010, **22**, 535–539.
12 C. Yu, K. Choi, L. Yin and J. C. Grunlan, *ACS Nano*, 2011, **5**, 7885–7892.
13 C. Yu, Y. S. Kim, D. Kim and J. C. Grunlan, *Nano Lett.*, 2008, **8**, 4428–4432.
14 J. L. Blackburn, A. J. Ferguson, C. Cho and J. C. Grunlan, *Adv. Mater.*, 2018, **30**, 1704386.
15 N. Toshima, *Synth. Met.*, 2017, **225**, 3–21.

16 C. Yu, A. Murali, K. Choi and Y. Ryu, *Energy Environ. Sci.*, 2012, **5**, 9481–9486.
17 C. A. Hewitt, A. B. Kaiser, S. Roth, M. Craps, R. Czerw and D. L. Carroll, *Nano Lett.*, 2012, **12**, 1307–1310.
18 J.-H. Bahk, H. Fang, K. Yazawa and A. Shakouri, *J. Mater. Chem. C*, 2015, **3**, 10362–10374.
19 D. Son, J. Lee, S. Qiao, R. Ghaffari, J. Kim, J. E. Lee, C. Song, S. J. Kim, D. J. Lee and S. W. Jun, *Nat. Nanotechnol.*, 2014, **9**, 397–404.
20 J. Heikenfeld, A. Jajack, J. Rogers, P. Gutruf, L. Tian, T. Pan, R. Li, M. Khine, J. Kim and J. Wang, *Lab Chip*, 2018, **18**, 217–248.
21 Z. Liang, L. Chen and G. C. Bazan, *Adv. Electron. Mater.*, 2019, **5**, 1900650.
22 K. Chatterjee, A. Negi, K. Kim, J. Liu and T. K. Ghosh, *ACS Appl. Energy Mater.*, 2020, **3**, 6929–6936.
23 B. Dörling, X. Rodríguez-Martínez, I. Álvarez-Corzo, J. S. Reparaz and M. Campoy-Quiles, *Appl. Phys. Lett.*, 2021, **118**, 213901.
24 P. G. Collins, K. Bradley, M. Ishigami and A. Zettl, *Science*, 2000, **287**, 1801–1804.
25 N. Toshima, K. Oshima, H. Anno, T. Nishinaka, S. Ichikawa, A. Iwata and Y. Shiraishi, *Adv. Mater.*, 2015, **27**, 2246–2251.
26 T. Fukumaru, T. Fujigaya and N. Nakashima, *Sci. Rep.*, 2015, **5**, 1–7.
27 Y. Nonoguchi, M. Nakano, T. Murayama, H. Hagino, S. Hama, K. Miyazaki, R. Matsubara, M. Nakamura and T. Kawai, *Adv. Funct. Mater.*, 2016, **26**, 3021–3028.
28 D. D. Freeman, K. Choi and C. Yu, *PLoS One*, 2012, **7**, e47822.
29 S. Horike, T. Fukushima, T. Saito, T. Kuchimura, Y. Koshiba, M. Morimoto and K. Ishida, *Mol. Syst. Des. Eng.*, 2017, **2**, 616–623.
30 Y. Nonoguchi, K. Ohashi, R. Kanazawa, K. Ashiba, K. Hata, T. Nakagawa, C. Adachi, T. Tanase and T. Kawai, *Sci. Rep.*, 2013, **3**, 1–7.
31 M. Massetti, F. Jiao, A. J. Ferguson, D. Zhao, K. Wijeratne, A. Würger, J. L. Blackburn, X. Crispin and S. Fabiano, *Chem. Rev.*, 2021, **121**, 12465–12547.
32 G. Wu, Z.-G. Zhang, Y. Li, C. Gao, X. Wang and G. Chen, *ACS Nano*, 2017, **11**, 5746–5752.
33 B. Dörling, J. D. Ryan, J. D. Craddock, A. Sorrentino, A. E. Basaty, A. Gomez, M. Garriga, E. Pereiro, J. E. Anthony and M. C. Weisenberger, *Adv. Mater.*, 2016, **28**, 2782–2789.
34 Y. Liu, M. Nitschke, L. Stepien, V. Khavrus, V. Bezugly and G. Cuniberti, *ACS Appl. Mater. Interfaces*, 2019, **11**, 21807–21814.
35 N. J. Stanton, R. Ihly, B. Norton-Baker, A. J. Ferguson and J. L. Blackburn, *Appl. Phys. Lett.*, 2021, **119**, 023302.
36 B. A. MacLeod, N. J. Stanton, I. E. Gould, D. Wesenberg, R. Ihly, Z. R. Owczarczyk, K. E. Hurst, C. S. Fewox, C. N. Folmar and K. H. Hughes, *Energy Environ. Sci.*, 2017, **10**, 2168–2179.
37 W. Cacheris, S. Nickle and A. Sherry, *Inorg. Chem.*, 1987, **26**, 958–960.
38 A. Bencini, A. Bianchi, P. Dapporto, E. Garcia-Espana, V. Marcelino, M. Micheloni, P. Paoletti and P. Paoli, *Inorg. Chem.*, 1990, **29**, 1716–1718.
39 E. Kimura, *Tetrahedron*, 1992, **48**, 6175–6217.
40 S. Hata, M. Kusada, S. Yasuda, Y. Du, Y. Shiraishi and N. Toshima, *Appl. Phys. Lett.*, 2021, **118**, 243904.
41 R. Chen, J. Tang, Y. Yan and Z. Liang, *Adv. Mater. Technol.*, 2020, **5**, 2000288.
42 S. Hata, T. Mihara, M. Shiraishi, Y. Yamaguchi, Y. Du, Y. Shiraishi and N. Toshima, *Jpn. J. Appl. Phys.*, 2020, **59**, SDDD05.
43 Y. Liu, Q. Dai, Y. Zhou, B. Li, X. Mao, C. Gao, Y. Gao, C. Pan, Q. Jiang and Y. Wu, *ACS Appl. Mater. Interfaces*, 2019, **11**, 29320–29329.
44 C. Gao, Y. Liu, Y. Gao, Y. Zhou, X. Zhou, X. Yin, C. Pan, C. Yang, H. Wang and G. Chen, *J. Mater. Chem. A*, 2018, **6**, 20161–20169.
45 Y. Nonoguchi, A. Tani, T. Ikeda, C. Goto, N. Tanifuji, R. M. Uda and T. Kawai, *Small*, 2017, **13**, 1603420.
46 K. Kobashi, S. Ata, T. Yamada, D. N. Futaba, T. Okazaki and K. Hata, *ACS Appl. Nano Mater.*, 2019, **2**, 4043–4047.
47 S. Hata, J. Tomotsu, M. Gotsubo, Y. Du, Y. Shiraishi and N. Toshima, *Polym. J.*, 2021, 1–6.
48 W. Zhou, Q. Fan, Q. Zhang, L. Cai, K. Li, X. Gu, F. Yang, N. Zhang, Y. Wang and H. Liu, *Nat. Commun.*, 2017, **8**, 1–9.
49 C. Rao and R. Voggu, *Mater. Today*, 2010, **13**, 34–40.
50 P. Job, *Ann. Chim.*, 1928, **9**, 113–203.
51 M. Saleem and K.-H. Lee, *J. Lumin.*, 2014, **145**, 843–848.
52 E. Kimura, *Acc. Chem. Res.*, 2001, **34**, 171–179.
53 M. Wong, M. Paramsothy, X. Xu, Y. Ren, S. Li and K. Liao, *Polymer*, 2003, **44**, 7757–7764.
54 O. Bubnova, Z. U. Khan, H. Wang, S. Braun, D. R. Evans, M. Fabretto, P. Hojati-Talemi, D. Dagnelund, J.-B. Arlin and Y. H. Geerts, *Nat. Mater.*, 2014, **13**, 190–194.
55 J. Kong, N. R. Franklin, C. Zhou, M. G. Chapline, S. Peng, K. Cho and H. Dai, *Science*, 2000, **287**, 622–625.
56 V. Schroeder, S. Savagatrup, M. He, S. Lin and T. M. Swager, *Chem. Rev.*, 2018, **119**, 599–663.
57 C. J. An, Y. H. Kang, H. Song, Y. Jeong and S. Y. Cho, *J. Mater. Chem. A*, 2017, **5**, 15631–15639.
58 X. Nie, X. Mao, X. Li, J. Wu, Y. Liu, B. Li, L. Xiang, C. Gao, Y. Xie and L. Wang, *Chem. Eng. J.*, 2021, **421**, 129718.
59 S. Qin, J. Tan, J. Qin, J. Luo, J. Jin, S. Huang, L. Wang and D. Liu, *Adv. Electron. Mater.*, 2021, **194**, 2100557.
60 Y. Wang, Z. Chen, H. Huang, D. Wang, D. Liu and L. Wang, *J. Mater. Chem. A*, 2020, **8**, 24675–24684.
61 M. Sheng, Y. Wang, C. Liu, Y. Xiao, P. Zhu and Y. Deng, *Carbon*, 2020, **158**, 802–807.
62 X. Cheng, X. Wang and G. Chen, *J. Mater. Chem. A*, 2018, **6**, 19030–19037.
63 L. Wang, Z. Zhang, L. Geng, T. Yuan, Y. Liu, J. Guo, L. Fang, J. Qiu and S. Wang, *Energy Environ. Sci.*, 2018, **11**, 1307–1317.
64 R. Tian, C. Wan, Y. Wang, Q. Wei, T. Ishida, A. Yamamoto, A. Tsuruta, W. Shin, S. Li and K. Koumoto, *J. Mater. Chem. A*, 2017, **5**, 564–570.
65 G. Wu, C. Gao, G. Chen, X. Wang and H. Wang, *J. Mater. Chem. A*, 2016, **4**, 14187–14193.
66 C.-K. Mai, B. Russ, S. L. Fronk, N. Hu, M. B. Chan-Park, J. J. Urban, R. A. Segalman, M. L. Chabinyc and G. C. Bazan, *Energy Environ. Sci.*, 2015, **8**, 2341–2346.